ELEVENTH EUROPEAN ROTORCRAFT FORUM

Paper No. 31

APPLIED AERODYNAMICS OF CIRCULATION CONTROL AIRFOILS AND ROTORS

Ernest O. Rogers, Alan W. Schwartz, and Jane S. Abramson
David W. Taylor Naval Ship Research and Development Center
Bethesda, Maryland, USA

September 10-13, 1985
London, England

THE CITY UNIVERSITY, LONDON, EC1V OHB, ENGLAND

APPLIED AERODYNAMICS OF CIRCULATION CONTROL AIRFOILS AND ROTORS

Ernest O. Rogers, Alan W. Schwartz, and Jane S. Abramson
Aerospace Engineers
David W. Taylor Naval Ship Research and Development Center
Bethesda, Maryland, USA

ABSTRACT

The basic attribute of circulation control airfoils is high-lift capability with reduced dependence on dynamic pressure and angle of attack for production of that lift. Furthermore, if the airfoil is dual-slotted (bidirectional), performance is independent of flow direction. These capabilities make a lifting stoppable rotor aerodynamically feasible. For such a rotor, the critical flight condition (minimum available lift) occurs in the advance ratio range of 0.85 to 1.10 as a result of the trends in mean dynamic pressure on the retreating side. Analysis of the aerodynamic flow field for each blade element at the critical flight condition indicates that the airfoils operate, on a mean basis, in a low-speed ($M_\infty = 0.25$), highly yawed (40 deg) environment at a negative angle of attack (−2.5 deg.). Such information provides guidelines for properly designing airfoils and assessing their performance. Recent tests of circulation control airfoils have more clearly defined the stall boundaries and the influence of airfoil geometry on the optimal operating conditions. The increasing knowledge of both rotor and airfoil aerodynamics will be the basis for more advanced circulation control rotors through the integration of airfoil and rotor design.

1. INTRODUCTION

Airfoils that employ circulation control (CC) by means of a tangential wall jet ejected over a rounded trailing edge have unique performance characteristics that can greatly extend rotorcraft operating capabilities. Successful development of rotary wing V/STOL concepts that exploit this form of boundary layer control requires careful consideration of the basic aerodynamic properties of both CC airfoils and the rotors that employ them—properties which, in many cases, are substantially different from those of conventional technology. This paper presents an overview of the basic performance features of CC airfoils, their operating aerodynamic environment on high-speed rotors, and the relationship between airfoil and rotor design requirements. Discussion of airfoil performance characteristics is based on the results of recent investigations in transonic wind tunnels.

2. BASIC AIRFOIL CAPABILITIES

In addition to angle of attack, the operating state of a CC airfoil is specified by the level of boundary layer control, which is expressed by the coefficient of jet momentum

$$C_\mu = \dot{m} V_j/(qc)$$

By convention, the jet velocity (V_j) is calculated based on isentropic expansion from duct pressure (P_d) to free-stream static pressure (P_∞). Mass flow rate ($\dot{m}$) is similarly calculated; for experimental investigations, the measured value is used.

Because the jet momentum coefficient is the basic performance control parameter, it is instructive to examine other expressions for C_μ to obtain insight into its functional dependence. For incompressible flow,

*Presented at the 11th European Rotorcraft Forum, London, England, September 1985. (Revision of paper presented to the 41st Annual Forum of the AHS, May 1985.)

a convenient equation for C_μ is

$$C_\mu = 2(h/c)(\Delta P_d)/q$$

where h/c is slot height-to-chord ratio (typically 0.0020), and ΔP_d is duct gage pressure ($P_d - P_\infty$). This particular expression, which is accurate to within 25 percent for unchoked flow conditions, illustrates the essentially linear relationship between C_μ, duct pressure, and slot height. Observe that if the slot height is a function of duct pressure, due to structural deflection, a nonlinear C_μ versus P_d relationship develops. Another expression for C_μ, valid for unchoked compressible flow,

$$C_\mu = 2(h/c)(M_j/M_\infty)^2 \qquad (\text{for } M_j<1)$$

is helpful in recognizing potential sources of compressibility effects on performance.

Of considerable importance to flight applications is the level of C_μ that can be produced by a practical airborne air supply system. The peak level of duct pressure available on a flight vehicle is determined by several factors including the temperature rise through the compressor and the compressor weight. Pressure ratios (P_d/P_∞) of up to 2.4 are considered quite feasible. The slot height-to-chord ratio should not generally exceed 0.0020 due to airfoil efficiency considerations. For a pressure ratio of 2.1, the obtainable C_μ level as a function of Mach number is shown in Fig. 1. With increasing Mach number, the available C_μ declines by over two orders of magnitude due to the dynamic pressure term (q) in the denominator. This dependence of C_μ on q (or Mach number M_∞) can be regarded as the most basic influence of free-stream velocity on CC airfoil performance capabilities.

Figure 2 illustrates the basic performance attributes of CC airfoils. Very high lift coefficients (>4 in this case, >6 for other contours) are achievable at low Mach number where high C_μ is available and any adverse effects of locally supersonic flow can be avoided. At the higher C_μ levels, the lift due to blowing (ΔC_ℓ) is essentially proportional to the square root of C_μ; thus,

$$\Delta C_\ell = A\sqrt{C_\mu} + B$$

This functional relationship means that the lift force (ΔL) has a dependency not on V_∞^2 as with conventional airfoils but rather on V_∞ directly, through the q term in the basic C_μ equation. Consequently, for a given duct pressure, there is a reduced sensitivity of lift to changes in dynamic pressure ($q = 1/2\,\rho V_\infty^2$) for CC airfoils. In addition, throttling of the duct flow permits control of lift independently of changes in angle of attack. If a slot and separate supply duct are also placed at the leading edge, either end can function as the blown aerodynamic trailing edge by redirecting the air supply (single slot blowing according to external flow direction) or by operating both slots simultaneously (dual blowing).

3. HIGH-SPEED ROTOR APPLICATIONS

Circulation control technology is especially applicable to high advance ratio rotorcraft where the forward velocity approaches the rotational tip speed ($\mu = V_\infty/V_t > 0.5$). This results in large regions of reversed flow being encountered by the rotor blades. Conventional rotorcraft, lacking the ability to produce lift in or near the reverse flow region, are essentially limited to an advance ratio of 0.4. Cheeseman and Seed[1] observed that by blowing through the blade's leading edge slot when in the reverse flow region, a rotor can be fully trimmed through much higher advance ratios. This capability of CC airfoils to produce high lift independent of local flow direction makes a lifting stoppable ($\mu \to \infty$) rotor aerodynamically feasible. Thus, only a single lift system is required for such a V/STOL concept because the blades become high aspect ratio, crossed oblique wings for high-speed cruise. Simple nonrotating valving in the rotor head provides for dual or reversed-slot blowing, as well as for cyclic modulation of duct pressure required for rotor moment trim. Figure 3 explicitly illustrates dual slot CC operation in a partly reversed flow field with a strobed photograph of tufted blades at advance ratio $\mu = 0.70$. For the azimuth depicted, the relative flow direction has reversed at the 40-percent radius. There is no evidence of flow separation on the blade.

Operationally, the stoppable rotor V/STOL concept involves taking off in a rotary mode and, while maintaining a constant rotor rotational rate, accelerating to the flight speed where conversion to the fixed-wing mode is to be performed (Fig. 4). Conversion flight speed (typically at 250 knots and 0.7 advance ratio) is largely limited by the advancing tip Mach number. Flight mode conversion would be accomplished by braking the rotor to a stop over a 15- to 30-sec period. Following conversion, the aircraft accelerates to cruise speed. The procedure is reversed to reenter the rotary mode. Note that operation over the advance ratio range of zero to infinity is experienced as shown in Fig. 4.

For the purposes of rotor/wing and vehicle design, the most critical flight condition must be identified. A basic indication of the critical condition, where the lifting capability is minimum, can be obtained by examining how the mean dynamic pressure on the lifting system varies over the flight regime.[2] This analysis is feasible because the lift that can be utilized from the advancing side of the rotor disc where the dynamic pressure is high is limited by the capability to produce an opposing roll moment on the retreating side where the dynamic pressure is much lower. Therefore, under the assumption that lift is related to dynamic pressure, the retreating side dynamic pressure variation will indicate relative rotor lifting capability for trimmed, level flight.

Figure 5 presents the results of integrating the local dynamic pressure over the retreating side for a variety of flight scenarios. If the full rotor rotational rate (100% RPM) is maintained through extreme advance ratios, supersonic tip speeds notwithstanding, the relative lifting capability is minimum at $\mu = 0.85$. (To simulate a conventional rotor with negligible lift in reverse flow, the assumption is made in the integration that $q = 0$ in that region. The available rotor lift is then found to decline continuously from hover without the recovery experienced with the bidirectional CC airfoils at $\mu = 0.85$.) As illustrated, if conversion is initiated below $\mu = 1.1$, the reduction in rotor rotational speed is accompanied by a decline in lifting capability during conversion until a recovery begins at μ of 1.1. Increasing the advance ratio for the initiation of conversion produces less drop-off in available lift. (Recall that lift due to blowing has approximately a $\sqrt{q}$ dependency; therefore, Fig. 5 overstates the sensitivity of the lifting potential of a CC rotor to dynamic pressure. The trends, however, are correct.) In practice, the advancing tip Mach number determines the upper limit of advance ratio for starting the conversion maneuver. More sophisticated analysis as well as experimental results have verified the conclusion that the 0.85 to 1.10 advance ratio range is the critical flight region for rotor design and compressor sizing. Of course, at any given advance ratio, the dynamic pressure will be higher if the rotational tip speed, and hence flight speed, is increased. This effect can be envisioned as an elevation of the curves in Fig. 5. Therefore, the critical advance ratio should be designed to occur at the highest possible rotary-wing flight speed.

Many facets of high-speed CC rotor and airfoil aerodynamics can be perceived by examining the rotor disc loading distribution at the critical advance ratio. Figure 6 shows a typical blade loading map for $\mu = 0.85$ as predicted for an isolated rotor using the methodology of Reference 3. Loading is concentrated in the fore and aft regions of the disc, with a significant contribution produced in the reverse flow region. The substantial nonuniformity of the loading is partly a result of the proximity of the rotor wake to the plane of rotation. For peak rotor efficiency at high speed, the disc incidence is in the range of 2 to 6 deg nose-up; propulsive force is from engine thrust. This incidence coincides with the general wake trajectory that, when combined with the numerous tip path crossovers characteristic of high advance ratios, results in substantial excursions in the induced velocities. The combination of angle of attack, jet momentum coefficient, and dynamic pressure variations requires the application of higher harmonic control to the basic cyclic modulation of blade duct pressure to maintain acceptable vibration levels during conversion. The blade fatigue loading can also be alleviated by this technique.

Also of interest is the large region of negative lift on the advancing side shown in Fig. 6. This download is necessitated by roll moment trim requirements because the retreating side alone cannot produce enough moment to balance that generated on the advancing side. The negative lift region is also the area of highest Mach number. One implication with regard to airfoil performance requirements is that there may be no

need to produce substantial lift at very high local velocities. This and other perspectives on airfoil requirements can be obtained from a more detailed study of the aerodynamic environment in which the blades operate.

4. AIRFOIL OPERATING ENVIRONMENT

As previously indicated, the aerodynamic operating environment of the high-speed rotor blade is characterized by extreme variations in angle of attack, blowing coefficient, Mach number, and other performance determining parameters. A means of analytically prioritizing and summarizing the airfoil operating conditions has been developed to assess airfoil performance and to provide guidelines for design improvement. This procedure is essentially a statistical analysis of the aerodynamic operating conditions at each of the rotor blade segments. Parameters such as angle of attack, yawed flow angle, and lift coefficient are averaged either over a full revolution or only on the retreating side. In calculating these averages, it is imperative that the relative contribution of each rotor element location (ψ,r) to the overall rotor lift be considered. This can be done through weighting each parameter to be averaged by the absolute magnitude of the locally generated load. This load may be either the increment produced by blowing (the augmented lift) or the total loading, which includes the contributions of camber and angle of attack. Such a weighting concept reduces the influence of extreme conditions that offer little contribution to lift (α = 40 deg, for example) while inherently emphasizing the conditions with the highest payoff. Thus, the mean *productive* incidence, Mach number, etc., of each blade station can be identified in order to optimize rotor performance through a careful matching of airfoil capabilities and blade requirements. Such an analysis has been conducted for a typical, fully trimmed conversion flight condition at 200 knots. This is the same condition for which the disc loading map is presented in Fig. 6.

Of initial interest in Fig. 7A is the spanwise variation for the averaged loading. This information is obtained by integrating the local blade loading as expressed in pounds of lift per foot of span over a full revolution for each blade station. The rotor blade in this case has a constant chord with no taper. The component of load produced by blowing is relatively constant along the span with the inboard and outboard portions having nearly identical contributions. Viewed in terms of total (net) load, the inboard section carries substantially more load than the outer regions. The magnitude of the inboard loading implies the existence of strong root vorticies or alternatively, there is the design potential for significant hub/fuselage lift carryover.

The mean angle of attack is largely invariant with span position; see Fig. 7A. The negative values (−3 deg) are characteristic of CC rotors in forward flight partly because blade incidence (collective angle) must be kept low to prevent excessive roll moment from developing in the regions of high dynamic pressure on the advancing side. As presently implemented, CC cannot reduce the C_ℓ below the unblown value, and there is no cyclic variation of blade incidence on present CC rotor concepts. In any case, there is no difficulty in operating the airfoils in the 0 to −10 deg range. In fact, at low speed, depending on thickness ratio, more lift may be available at negative incidence than at positive incidence as will become apparent in the airfoil performance discussions to follow. As expected, there is a strong spanwise variation in Mach number. Peak levels vary from M = 0.35 inboard to 0.64 at the tip, whereas the load-weighted values are only 0.20 and 0.37, respectively.

Yawed flow conditions are examined by azimuthally averaging the weighted, absolute value of the local in-plane flow angles. Perhaps unexpectedly, mean flow angles between 35 and 40 deg (where 90 deg corresponds to flow down the span) are found over the full blade (Fig. 7A). The explanation is that substantial lift is produced in the fore and aft regions of the disc where the flight velocity vector is aligned with the blade.

The statistical analysis approach can be extended a step further. Instead of finding the average conditions at each blade station, the proportion of total rotor lift generated within specified Mach number or incidence ranges is determined. Thus, a distribution is obtained of loading versus the aerodynamic conditions under which the loading was produced. Again, such information contributes in identifying desirable airfoil properties.

In Fig. 7B, both the full disc and the retreating side of the disc are considered separately with regard to the distribution of blade loading. For the entire disc, the load is concentrated at low Mach number (0.15 to 0.25), with a nearly linear decline to the advancing tip Mach number of 0.64. This trend is not a result of any inability of a CC airfoil to produce lift at high Mach number; simply, for this application, there is no requirement to do so. For higher design rotational tip speeds—and possibly for other flight conditions as well—there will be more demand for lift at high local speed than is indicated in this sample case. The retreating side (Fig. 7B) has an even greater concentration of lift in the low-speed range with 80 percent of the total lift produced below M = 0.25.

When angle of attack is analyzed over the entire disc it is found that 50 percent of rotor lift is generated where local conditions result in a flow incidence of between 0 and −5 deg. Approximately 75 percent of rotor lift occurs in the negative incidence ranges. A more extreme variation is found on the retreating side with angles of less than −10 deg providing substantial contributions to rotor performance.

This analysis has emphasized lift rather than aerodynamic drag, because at high advance ratios rotor shaft power is much less than the compressor power required to produce lift. At other flight conditions, blade section drag would be a prime subject for analysis.

The concept of a weighted, statistical analysis of a widely varying aerodynamic environment should have application to conventional rotorcraft was well. The analysis can be extended to cover a complete flight scenario (time averaging) thereby providing a more comprehensive identification of airfoil/blade requirements. A further extension of this technique would automate the rotor/airfoil design process by adding logic to rotor performance codes for altering airfoil contours (and performance representation) in accordance with operating environment statistics.

In summary, at the critical flight condition examined here (μ = 0.85), 56 percent of rotor lift is generated on the retreating side where the mean productive incidence is −3 deg at a Mach number of 0.17; the corresponding lift coefficient is 2.9. For the complete disc, the average conditions are α = −2.5 deg, M = 0.27, C_μ = 0.09, and yawed flow angle of 38 deg. With this insight into the aerodynamic environment, the basic performance characteristics of CC airfoils can now be reviewed in proper perspective.

5. AIRFOIL PROPERTIES

Major geometric parameters unique to circulation control airfoils are shown in Fig. 8. Slot position is generally within 4-percent of the trailing edge as determined by the location of the adverse pressure gradient for representative operating conditions. Nozzle contouring contributes to the establishment of a tangential jet ejection angle. Downstream of the nozzle, the trailing edge radius and rate of change in curvature are determined by the requirement to maintain attached jet flow. The jet remains attached over the curved trailing edge surface due to the Coanda effect that results from a balance between centrifugal force and surface pressure. Entrainment of the upper surface flow results in the movement of the stagnation point toward the lower surface, thereby producing an increase in circulatory lift.

The fundamental manner in which various factors influence the airfoil pressure distribution is presented in Fig. 9. As with conventional airfoils, changing angle of attack moves only the location of the leading edge stagnation point thereby producing the highest incremental loading in the leading edge region. This effect occurs independently of the blowing level. The center of loading due to angle of attack, therefore, is at the quarter chord. If trailing edge blowing is increased with incidence held fixed, then not only does the trailing edge stagnation point move further onto the lower surface but also the leading edge point moves an equal amount. The net result is increased loading at both ends of the chord and the center of pressure due to CC is at midchord.

The concentration of chordwise load at the leading edge may result in leading edge separation due to severe adverse pressure gradients ("thin airfoil" stall). To remedy this, camber and thickness are used to partly shift the loading to midchord. There is, however, a practical limit to the use of camber or thickness for this purpose because of the adverse pressure gradients that would exist upstream of the slot at low lift coefficients ("thick airfoil" stall). A representative pressure distribution for a CC airfoil is shown in Fig. 9D. The ability to carry load over the full chord length is a fundamental advantage of blown airfoils.

One effect of compressibility is to alter the upper surface pressure distribution (Fig. 10) in a manner analogous to that produced by increasing thickness or camber. This effect of compressibility is nothing more than that modeled by the familiar transonic similarity rules. The result, however, is more dramatic for CC airfoils because of the relatively high thickness and camber used and the influence that the upstream pressure gradient has on performance.

6. AIRFOIL PERFORMANCE

The following overview of airfoil characteristics applies when using trailing edge blowing only.

6.1 Lift

At low speed, basic airfoil performance in terms of C_ℓ versus angle of attack at constant C_μ, as shown in Fig. 11 for $M_\infty = 0.12$, resembles that of a conventional flapped airfoil. Substantial lift is available even at a -15 deg incidence. At any blowing level, lift increases with incidence until a stall point is reached, defined here as $\partial C_\ell / \partial \alpha = 0$ and referred to as angle of attack or "alpha" stall. Alpha stall is generally a result of high leading edge pressure gradients causing flow separation. These gradients can be reduced for a given C_ℓ by decreasing the incidence and increasing the blowing coefficient. The net result, depending on leading edge radius, is that a higher lift may be achieved at more negative incidence through aft loading—if the only stall phenomena present is upper surface flow separation.

If a relatively thick airfoil is selected, other angle-of-attack related phenomena are observed. For very low blowing levels, as angle of attack is increased, an adverse pressure gradient develops ahead of the slot. Such a gradient results in either a large boundary layer deficit or an aft flow separation, both of which reduce airfoil lifting efficiency (defined as $\partial C_\ell / \partial C_\mu$ and called augmentation ratio). With sufficient Coanda blowing, augmentation returns to expected levels indicating that a decrease in the boundary layer deficit or flow reattachment has occurred.

At other than very low speed ($M_\infty < 0.2$), compressibility influences performance because of the high surface velocities inherent in high-lift production. Figure 12 shows the high-speed performance of a CC airfoil ($t/c = 0.16$) at zero incidence for the 0.3 to 0.8 Mach number range. Blowing has the capability to increment lift even at $M_\infty = 0.8$, where shock waves are present on both upper and lower surfaces. The two major effects of M_∞ on the lift coefficient readily apparent from these data are a reduction in maximum lift coefficient and a reduction in augmentation ratio.

Within the Mach number range shown, C_ℓ is limited by "C_μ" stall ($\partial C_\ell / \partial C_\mu = 0$), which has been found to correlate with the attainment of the critical pressure coefficient (C_p^*) on the Coanda surface.[4] Note that although C_p^* is defined as the static pressure corresponding to sonic flow, this value on the Coanda surface does not necessarily imply anything about the jet Mach number. There is no correlation of any changes in performance uniquely associated with attaining a choked jet ($M_j = 1.0$) condition. Indeed, successful operation at jet Mach numbers up to 1.4 has been demonstrated.[4] The initial appearance of C_p^* on other than the trailing edge region does not have an influence on performance. Airfoil pressure distributions at or beyond "C_p^*" stall do not indicate flow separation or shock waves (Fig. 13). The pressure distribution matches that predicted by inviscid analysis, thus confirming that strong viscous phenomena of the type

associated with conventional stall have not occurred. In fact, potential flow is used to accurately predict the C_ℓ-α-M_∞ conditions at which a given airfoil design will reach this particular lift limit. The exact physical phenomenon responsible for the C_p^* related stall has yet to be identified, but is presumably associated with supersonic flow effects originating in the flow field just exterior to the jet.

The onset of stall (Fig. 12) at lower C_μ levels as M_∞ increases parallels the trends in available C_μ (Fig. 1). Therefore, in terms of duct pressure ratio, stall is no more likely to occur at higher Mach numbers than at lower free-stream velocities (Fig. 14). Also, it is important to be aware that although C_ℓ declines with M_∞, the actual lift function (C_ℓ q or $C_\ell M_\infty^2$) continues to increase through M = 0.6 for this particular airfoil; and, of course, lift due to incidence is additive to these force levels.

As stated, the second major effect of compressibility is a reduction in lifting efficiency (augmentation ratio). For the 103RE airfoil, this effect can be seen at M_∞ of 0.6 and 0.7 in Fig. 12 where the flow is still completely subsonic. The decrease in efficiency is a direct result of an aft pressure gradient brought about by the compressibility effect depicted in Fig. 10. This adverse gradient is analogous to that experienced at low subsonic speeds when thick or highly cambered airfoils operate at positive incidence. Again, the increased boundary layer momentum deficit requires an increase in jet momentum for a given increment in lift. Figure 15 shows the experimental correlation of adverse gradient just upstream of the slot with Mach number and blowing requirements for constant lift. Altering airfoil camber or thickness changes the Mach number at which the adverse gradient is severe enough to decrease efficiency. In general, pressure distributions likely to reduce augmentation ratio are identifiable with standard inviscid airfoil theory.

An example of how geometry influences basic performance can be seen in a summary of data from recent airfoil tests in transonic wind tunnels. Lift control capabilities at constant incidence, $\Delta C_\ell = (C_{\ell max} - C_{\ell min})_{\alpha=0}$, are plotted in Fig. 16 using logarithmic scales developed so that any phenomenon directly related to C_p^* (sonic flow pressure) will appear as a straight line. For reference, the stall limit of the NACA 0012 airfoil is shown. The corresponding maximum achievable lift of the CC airfoils is not shown in the figure because lift due to incidence is not included. Increasing the thickness and camber to chord ratios from the respective values of 0.16 and 0.01 on the 103RE airfoil to 0.20 and 0.03 on the 20/3 model enhances low speed performance.

When viewed not in terms of ΔC_ℓ but rather as a function more directly related to lift force ($\Delta C_\ell M_\infty^2$), the influence of geometry on maximum performance is quite revealing. The series of airfoils (t/c from 0.15 to 0.21) in Fig. 17 constitute a geometric family in that their basic contour parameters are the same linear functions of the thickness ratio. Remarkably, all four sections have the same peak value of the lift function, and differ only in the Mach number at which the peak occurs. As is apparent, the performance data of these four airfoils can be collapsed into a single curve with proper flow and geometry similarity parameters. Such parameters are currently under analytical and empirical development. These similarity relationships are expected not only to contribute to the development of advanced CC airfoils but also to define their optimum placement on the rotor blade.

One perspective on the interrelationship of airfoil performance traits and rotor requirements is illustrated in Fig. 18. If the airfoils in Fig. 17 are used to define a rotor blade which varies linearly in blade section thickness ratio, the airfoil loading capability ($\Delta C_\ell q$) reaches a maximum in the fore and aft disc regions for the flight speed of 250 knots. As stated, this location of peak loading is optimal for the critical flight condition because roll moment trim requirements prohibit full utilization of airfoil lifting capability elsewhere on the advancing side. Thus one obvious consideration for a balanced rotor/airfoil design is a matching of rotor rotational speed and spanwise variation in airfoil contour.

6.2 Drag

Using a momentum deficit method, drag is calculated from experimental measurements taken with a wake rake. Because this method does not account for the momentum introduced by the jet, a correction term must be applied to $C_{d_{rake}}$. The modified drag coefficient $C_d = C_{d_{rake}} - C_\mu V_\infty/V_j$ is shown for three airfoils in Fig. 19. These three airfoils share a common profile but have distinctly different Coanda surface geometries; see Ref. 4 for complete airfoil description. It is obvious from the results in Fig. 19 that factors which depend on trailing edge geometry, such as base pressure and jet momentum thrust recovery, have a strong influence on drag levels. The LS trailing edge has the lowest unblown drag level and also the highest drag when blown. In contrast, the DE trailing edge has the highest unblown drag, but the lowest drag when blowing.

The effect of Mach number on drag at zero incidence is shown in Fig. 20. At low Mach numbers, drag can become negative due to thrust recovery from the higher available blowing coefficients. There is a general elevation in drag with increasing Mach number with $M_\infty = 0.8$ displaying the substantial drag rise expected from shock waves present at this speed. In addition, at constant M_∞ there is a drag rise associated with increasing C_ℓ followed by a decline just before maximum C_ℓ is reached. Several of the curves in Fig. 20 have been extended beyond the peak lift point. The immediate post stall drag behavior is seen to be that of rapid change, but it may be initially decreasing or increasing. Such nuances of the drag characteristics have yet to be fully investigated.

6.3 Pitching Moment

In Fig. 21 pitching moment ($C_{m_{1/2}}$) is plotted against lift coefficient for a representative symmetric airfoil. Moment is resolved about the half-chord because the elastic axis for a stoppable rotor blade would be at center chord. The moment is essentially independent of augmented lift level until maximum C_ℓ is approached, where the moment becomes more negative due to increased jet suction over the Coanda region. Mach number also has a minimal influence on the moment associated with lift due to blowing. Angle of attack is by far the dominant factor influencing midchord moment, because the center of lift for incidence is in the 20- to 30-percent chord range.

There are really two aerodynamic centers associated with CC airfoils corresponding to the individual effects of augmented lift and lift due to angle of attack. Figure 21 is plotted for a constant effective angle of attack (corrected for wind tunnel interference effects) so that the slope $\Delta C_{m_{1/2}}/\Delta C_\ell$ directly indicates the location of the blowing aerodynamic center with respect to midchord. This center is essentially at $x/c = 0.50$ (within 2-percent), as suggested by the theoretical pressure distribution of Fig. 9B. It is surprising that experimentally the center of pressure should be so close to midchord because the local suction pressure produced directly by the jet on the Coanda surface should shift the center aft. It appears that the moment produced directly by jet suction is largely offset by the loss of pressure in the separation region on the lower trailing edge near the location of the theoretical stagnation point (Fig. 13). Nonsymmetrical contours, however, may have an aft aerodynamic center. Additionally, an aft movement of the center may be produced by any circumstances that influence performance to the extent that an unusually high blowing level is required for a given ΔC_ℓ. Such an effect can be seen in Fig. 21 from the increased $\Delta C_{m_{1/2}}/\Delta C_\ell$ slope at the higher lift levels and at $M_\infty = 0.7$.

Fig. 22 addresses incidence effects directly with both C_ℓ and $C_{m_{1/2}}$ plotted against the effective angle of attack. The moment is a strong, linear function of the incidence over the -12 to $+$ 5-deg range of this data. At the blowing level shown, the $C_\ell - \alpha$ slope is 0.113 per deg. When combined with the C_m-α slope of 0.025 per deg, the aerodynamic center for angle of attack effects is at $x/c = 0.27$.

7. SUMMARY

Circulation control airfoils are capable of producing high lift with a reduced dependence on dynamic pressure. If the contours are dual-slotted, lift can be produced independently of flow direction. For a rotor employing CC airfoils, the critical flight condition (minimum available rotor lift) is in the advance ratio range of 0.85 to 1.1 where the mean dynamic pressure on the retreating side reaches a minimum. Above an advance ratio of 1.1, lifting capability increases rapidly thereby permitting a complete stopping of the rotor with the blades becoming high aspect ratio crossed oblique wings.

Analysis of the critical flight condition ($\mu = 0.85$) indicates that the mean aerodynamic operating condition for the blade airfoils is at negative angle of attack (−2.5 deg) and low Mach number (0.27), in a highly yawed flow field. There is little demand for production of lift in the regions of the disc with high local Mach number. Blade loading, azimuthally averaged, is highest inboard.

The lifting characteristics of current design CC airfoils are as follows: There is a basic $C_\ell - C_\mu$ response that is linear in the low C_μ range with C_ℓ versus C_μ slopes of up to 80 having been demonstrated over the t/c range of 0.15 to 0.21. At the higher C_μ levels available at low speed, the relationship with C_ℓ is $A\sqrt{C_\mu}$, where A is approximately 16. These efficiency factors decline under conditions where substantial adverse pressure gradients develop upstream of the slot. These conditions include positive incidence at low blowing levels and high Mach number for thick or highly cambered sections.

Response to angle of attack at constant blowing is the same as that of conventional airfoils, although alpha stall can occur at a much lower incidence under high-lift conditions. Lifting capability is bounded either by the availability of C_μ or by one of two types of stall: (1) alpha stall due to high leading edge pressure gradients causing flow separation, which is most likely to occur at low speed where high C_μ is available; and (2) compressibility induced C_μ stall that can occur above 0.2 M_∞ due to high trailing edge pressure peaks (local Mach number >1.0). Whether these limits are of concern is entirely application dependent. Airfoil geometry can be tailored to vary chordwise loading and thus alter the conditions at which these performance restrictions will occur. There are two aerodynamic centers: quarter-chord for lift due to incidence and midchord for lift due to blowing.

Inviscid airfoil analysis can identify many important performance trends and thereby provide a means of designing airfoils specifically tailored to operational requirements. Advances in fundamental operating efficiency, for example, drag and augmentation ratio, will depend upon the continued development of viscous-based computational methods.

8. CONCLUDING REMARKS

A high-speed stoppable rotor V/STOL vehicle is feasible because of the unique properties of circulation control airfoils. Similarly, the aerodynamic environment of high-speed rotors is unique. Thus, full exploitation of the CC rotor concept requires an integration of rotor and airfoil design, perhaps more so than for conventional lifting systems. It should be mentioned that current experimental blown rotors and their airfoils are first-generation designs developed before the recent advancements in understanding CC performance characteristics. The gains available from a properly tailored rotor/airfoil design should be substantial.

9. REFERENCES

1. Cheeseman, I.C. and Seed, A.R., "The Application of Circulation Control by Blowing to Helicopter Rotors," Journal of the Royal Aeronautical Society, Volume 71, July 1967.

2. Schwartz, A.W., "Basic Consideration of the Lifting Capability of Stoppable Rotors," DTNSRDC/ASED-84/10, Dec 1984.

3. Rogers, E.O., "Recent Progress in Performance Prediction of High Advance Ratio Circulation Controlled Rotors," Paper No. 29, Sixth European Rotorcraft and Powered Lift Aircraft Forum, Bristol, England, Sep 1980.

4. Abramson, J. and Rogers, E.O., "High-Speed Characteristics of Circulation Control Airfoils," Paper No. 83-0265, AIAA 21st Aerospace Sciences Meeting, Reno, Nevada, Jan 1983.

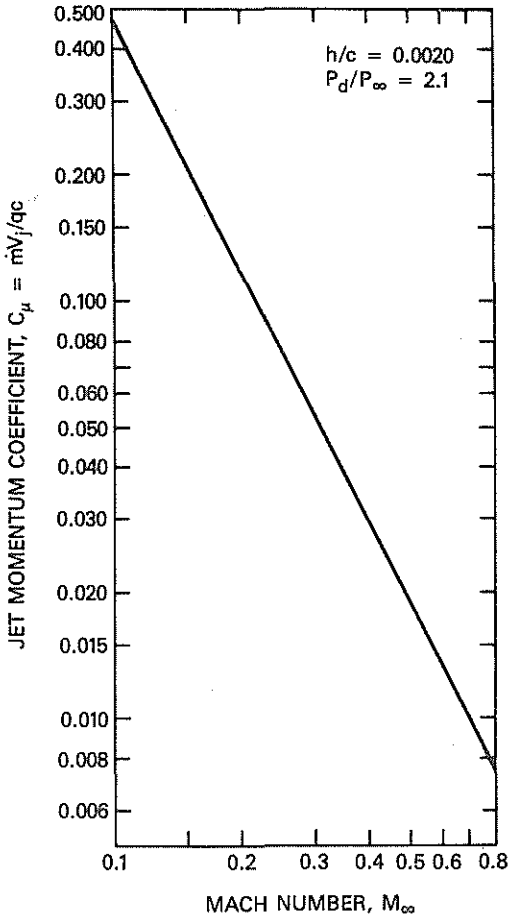

Fig. 1 Effect of Mach Number on the Maximum Available Momentum Coefficient, C_μ. (Typical)

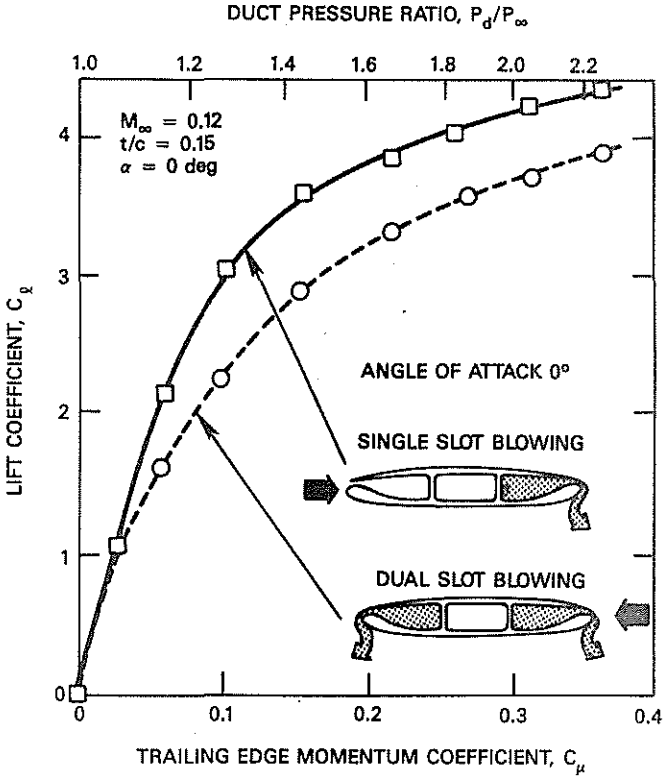

Fig. 2 Basic Performance Attributes of CC Airfoils.

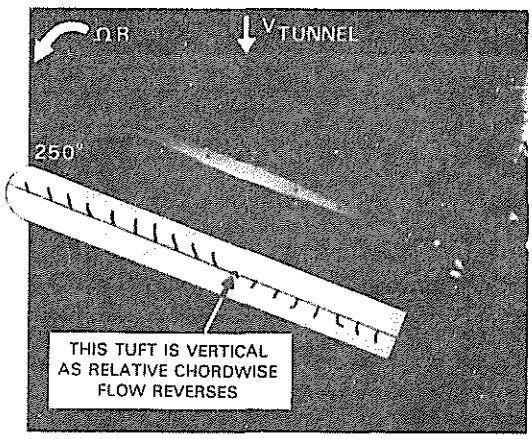

Fig. 3 Operation in a Partially Reversed Flow Region: Retreating Side Photograph of a Dual Blowing Tufted Blade at Advance Ratio of 0.7 (C_T/σ = 0.085, α_s = +2.5, θ_c = −4 deg).

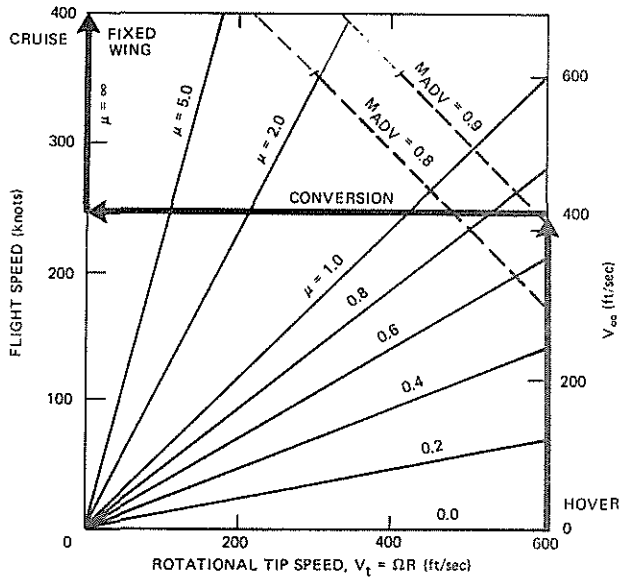

Fig. 4 Typical Rotary to Fixed Wing Flight Mode Conversion Scenario.

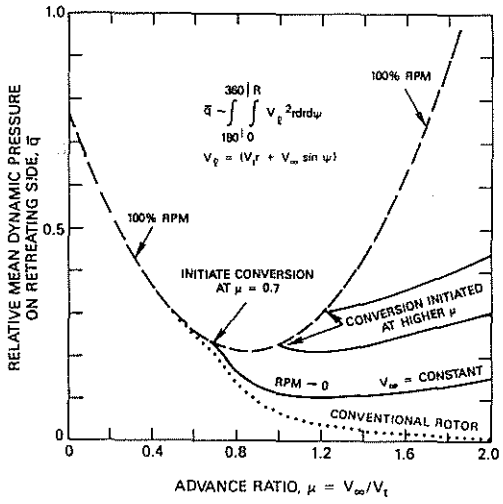

Fig. 5 Identification of Critical Flight Conditions: Retreating Side Mean Dynamic Pressure Behavior for Various Conversion Scenarios of a Stoppable Rotor.

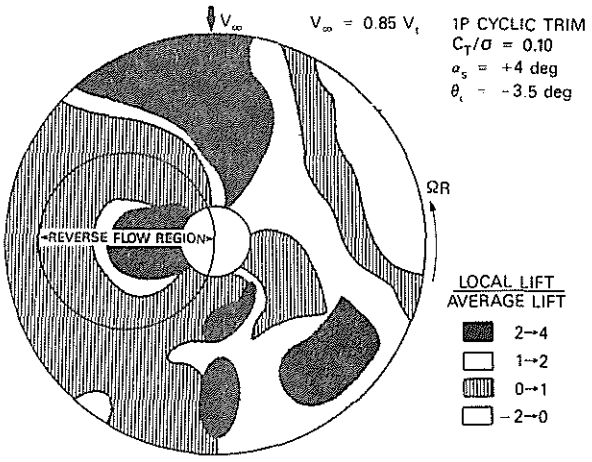

Fig. 6 Typical Load Distribution at Critical Flight Condition (Analytically Predicted).

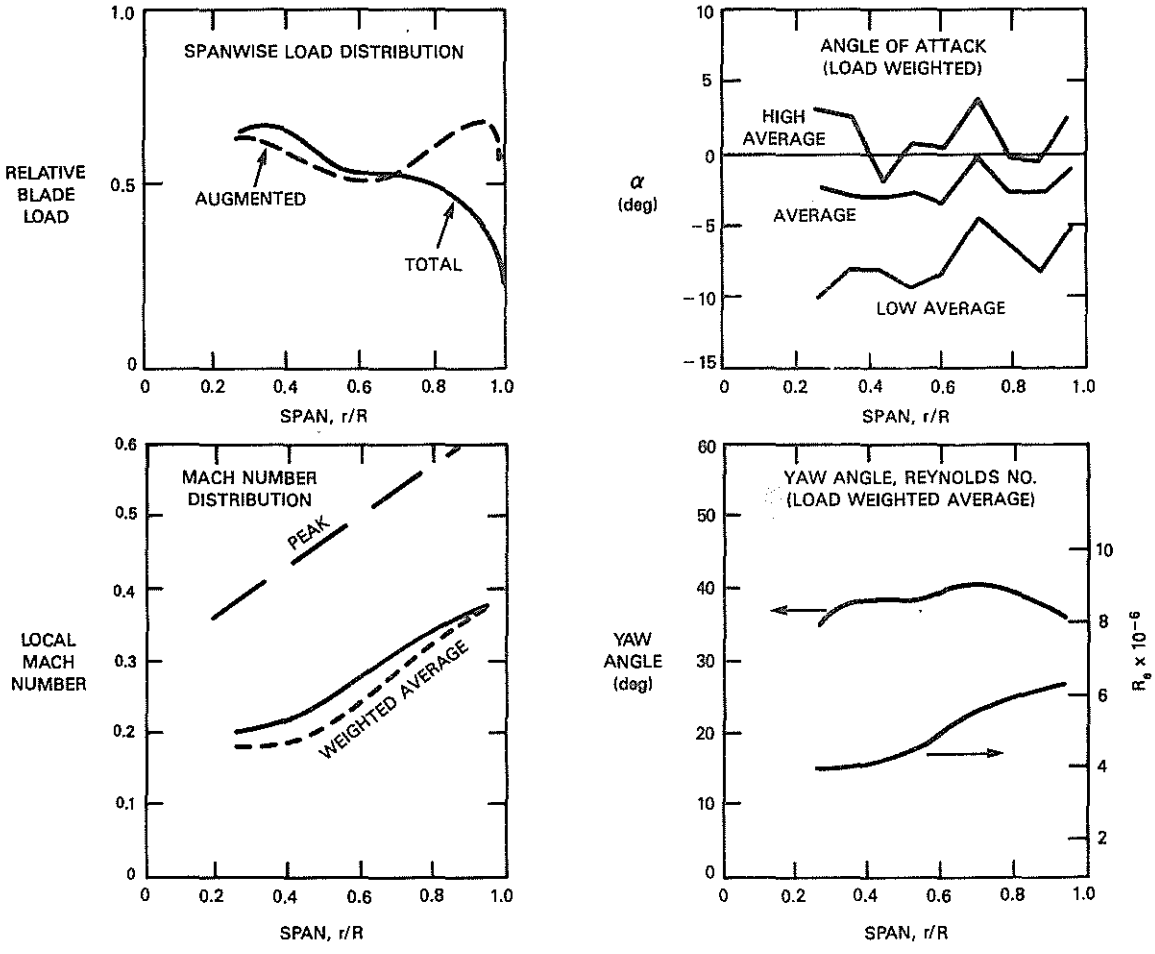

Fig. 7A Radial Distributions Averaged Over 0 to 360 Degrees.

Fig. 7 Airfoil Operating Environment at Critical Flight Condition (μ = 0.85).

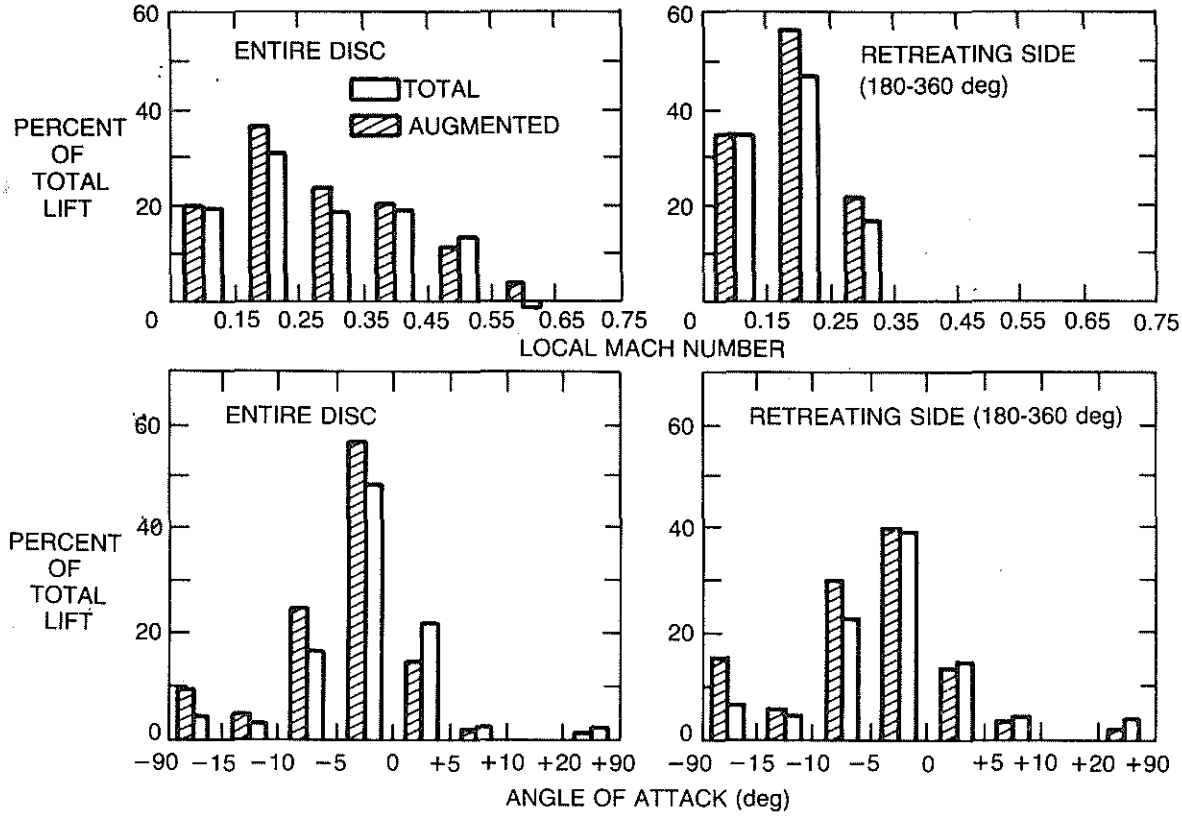

Fig. 7B Distribution of Blade Loading with Respect to Blade Section Mach Number and Angle of Attack.

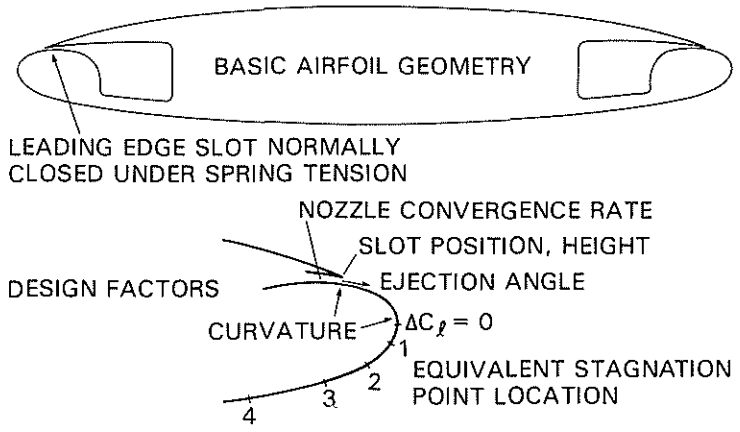

Fig. 8 Airfoil Design Parameters.

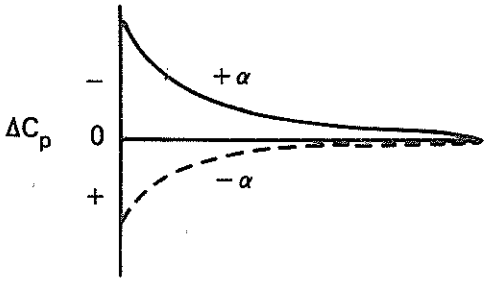

Fig. 9A Angle of Attack Effect: Movement of Leading Edge Stagnation Point.

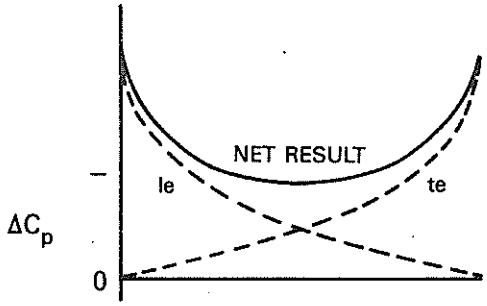

Fig. 9B CC Effect: Movement of Both Leading and Trailing Edge Stagnation Points.

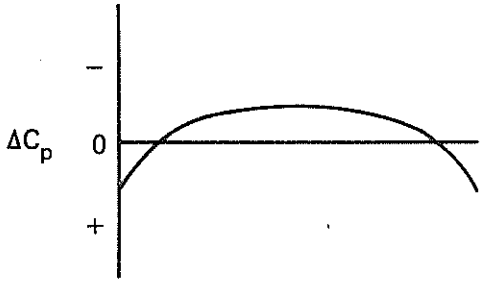

Fig. 9C Camber and Thickness Effect.

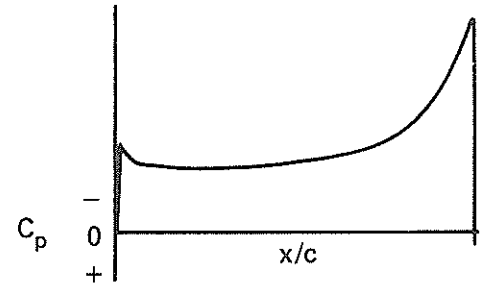

Fig. 9D Representative Net Results t/c = 0.18, δ/c = 0.03, $\alpha = -5°$, $C_\ell = 3.0$

Fig. 9 Basic Principles of CC Airfoils: Components of Upper Surface Pressure Distribution (With Boundary Layer Control at Trailing Edge).

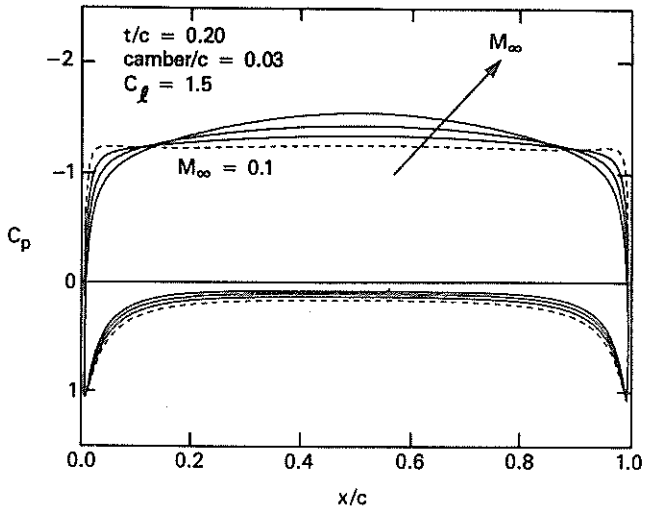

Fig. 10 Influence of Mach Number on Chordwise Pressure Distribution at Constant Lift.

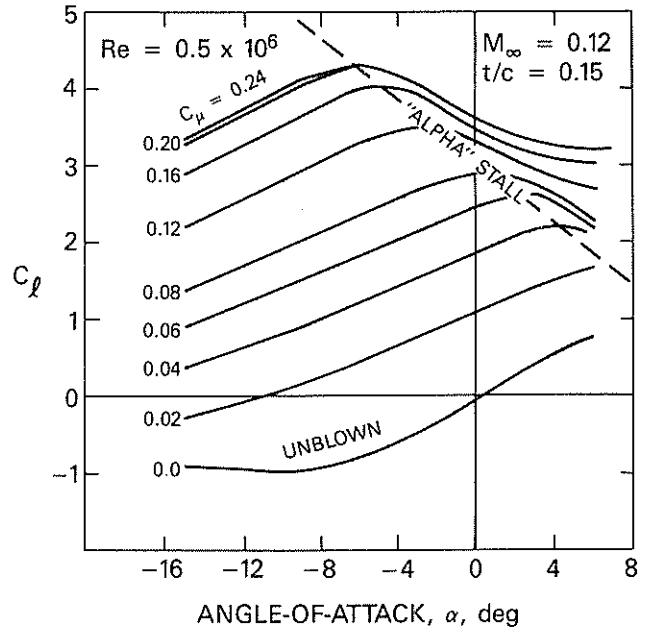

Fig. 11 Response to Angle of Attack at Constant Blowing.

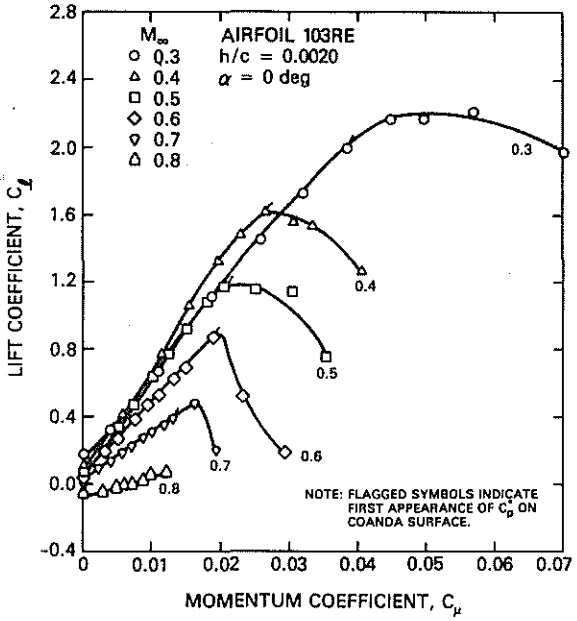

Fig. 12 Effects of Mach Number (Ref. 4).

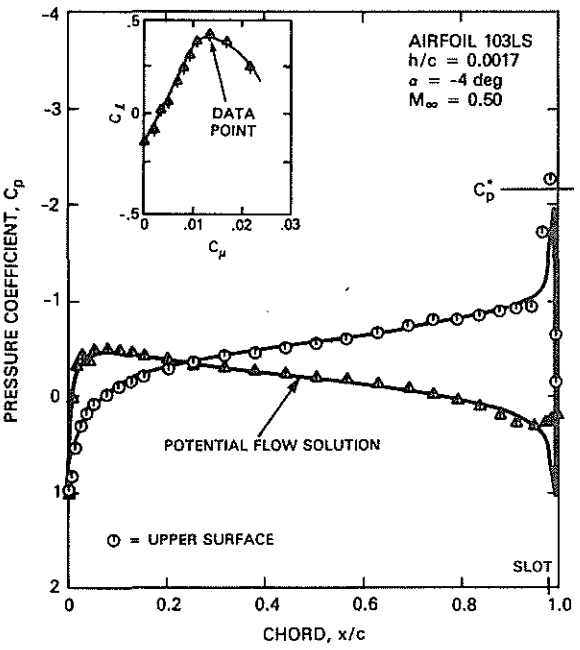

Fig. 13 Pressure Distribution at "C_μ" Stall Point Illustrating the Association of the Pressure Corresponding to Sonic Flow (C_p^*) with Stall.

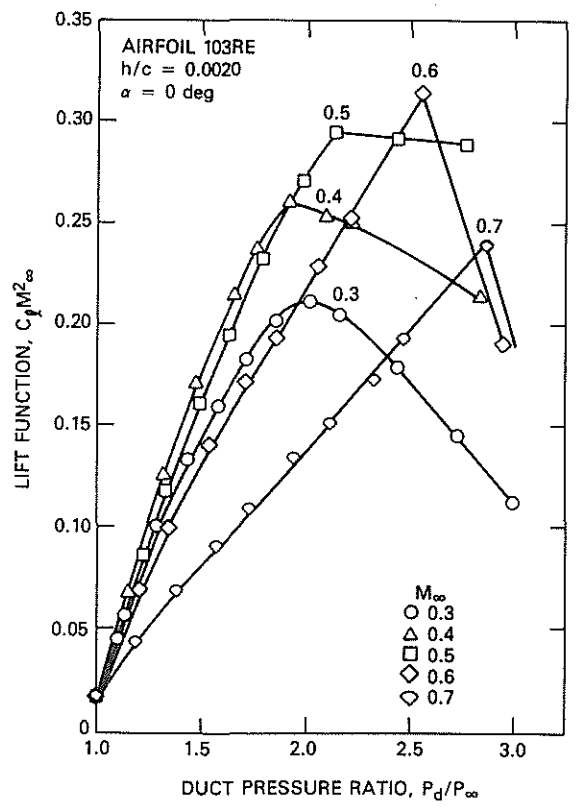

Fig. 14 Lift Function ($C_\ell M_\infty^2$) Versus Duct Pressure Ratio for Data Presented in Figure 12.

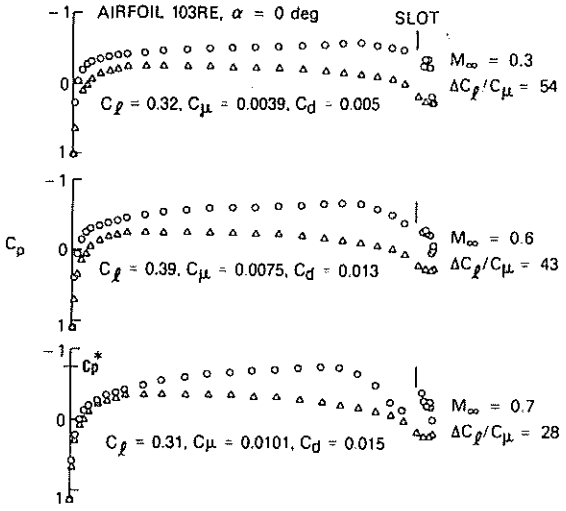

Fig. 15 Increase of Adverse Pressure Gradient Upstream of Slot with Increasing Mach Number at Essentially Constant C_ℓ.

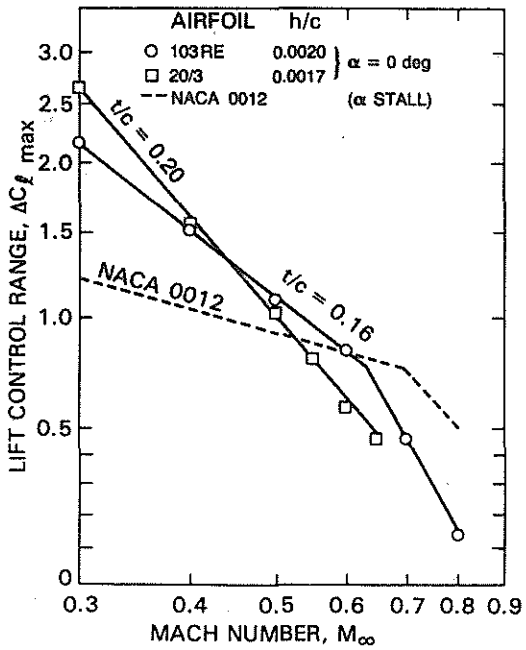

Fig. 16 Lift Coefficient Control Ranges of Two Representative CC Airfoils at Constant Incidence of Zero Degrees.

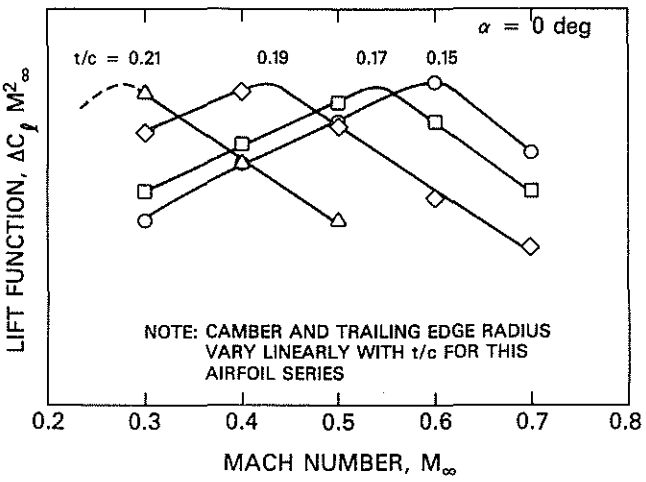

Fig. 17 Influence of Mach Number and Airfoil Geometry on Capability to Augment Loading at Zero Incidence.

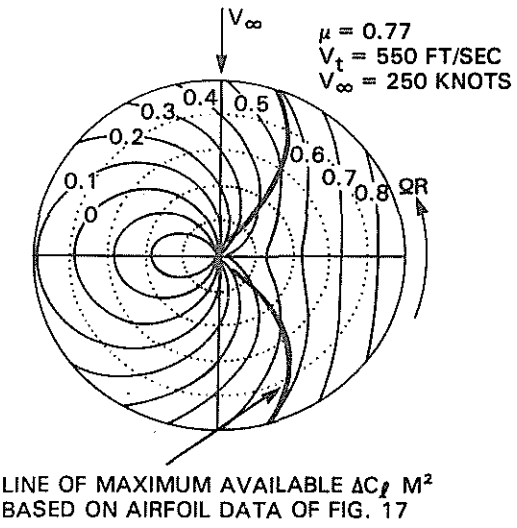

Fig. 18 Rotor Disc Mach Number Contours with Locus of Maximum Available Load for a Representative Rotor Design.

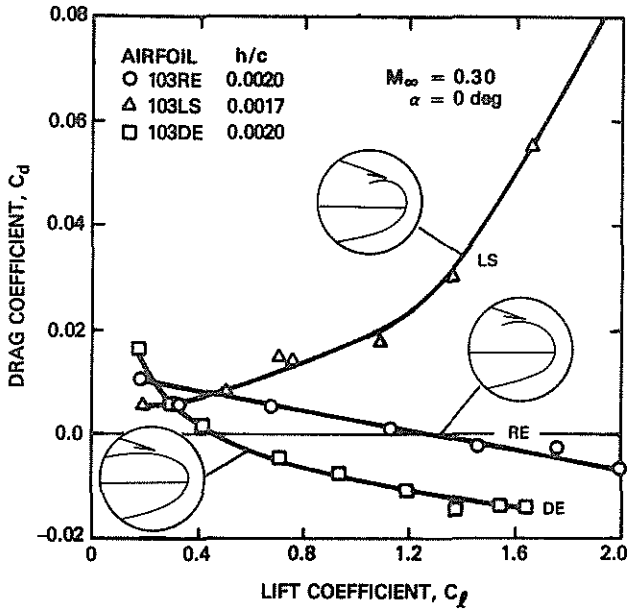

Fig. 19 Influence of Trailing Edge Design on Drag Coefficient.

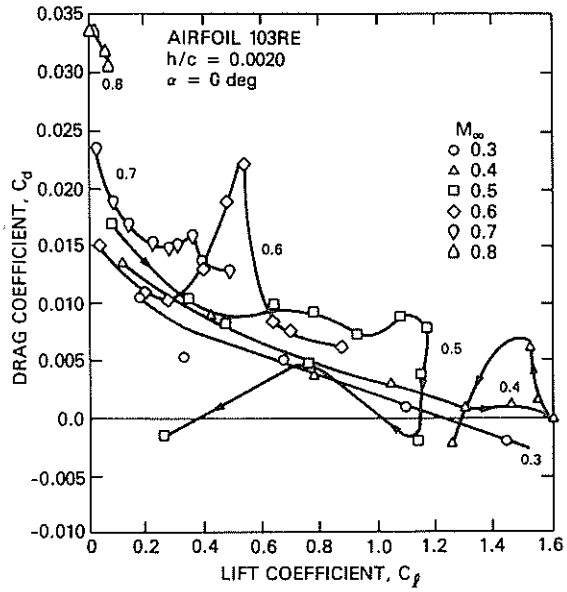

Fig. 20 Drag Variation with Lift Over a Mach Number Range.

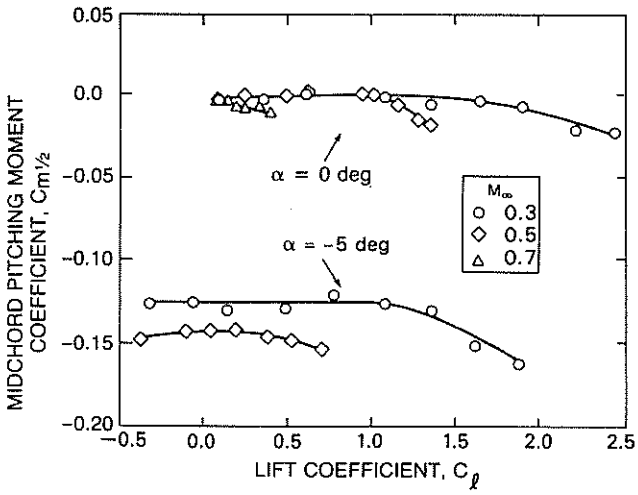

Fig. 21 Pitching Moment Coefficient About Midchord at Constant Effective Incidence.

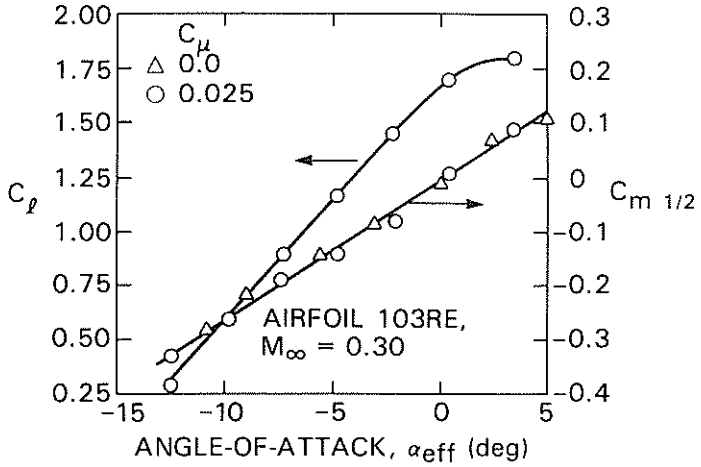

Fig. 22 Influence of Angle of Attack on Moment and Lift at Constant Blowing Conditions.